

I. Kandarakis
D. Cavouras

Experimental and theoretical assessment of the performance of $Gd_2O_2S:Tb$ and $La_2O_2S:Tb$ phosphors and $Gd_2O_2S:Tb-La_2O_2S:Tb$ mixtures for X-ray imaging

Received: 11 January 2000
Revised: 3 August 2000
Accepted: 14 September 2000
Published online: 20 February 2001
© Springer-Verlag 2001

I. Kandarakis · D. Cavouras (✉)
Department of Medical Instrumentation
Technology, Technological Educational
Institution of Athens, Ag. Spyridonos
Street, Aigaleo, 122 10 Athens, Greece
E-mail: cavouras@hol.gr
Phone: +30-1-5 38 53 72
Fax: +30-1-5 91 09 75

Present address:
D. Cavouras, 37-39 Esperidon Street,
Kallithea 17671, Athens, Greece

Abstract The purpose of this work was to investigate and compare the imaging performance of $Gd_2O_2S:Tb$ and $La_2O_2S:Tb$ phosphors as well as of $Gd_2O_2S:Tb$ and $La_2O_2S:Tb$ mixtures for use in X-ray imaging detectors (intensifying screens). Phosphors were supplied in powder form and were used to prepare test screens. Three types of screens were prepared: $Gd_2O_2S:Tb$; $(Gd_{50}La_{50})O_2S:Tb$; and $La_2O_2S:Tb$. Screens were excited by X-rays with tube voltages from 40 to 120 kV and their efficiency (light intensity or light energy flux over exposure) was measured with a photomultiplier and a dosimeter. The light spectrum was also measured with a monochromator. From these measurements, the number of emitted photons per incident X-ray (NEP) and the zero frequency detective quantum efficiency (DQE(0)) of the screens were determined. Additionally, modulation transfer function (MTF) was measured by the square wave response function (SWRF)

method. A theoretical model calculating NEP and DQE was also developed to fit experimental data and predict the performance of $Gd_2O_2S:Tb-La_2O_2S:Tb$ mixtures by weight from 10–90% to 90–10%. $Gd_2O_2S:Tb$ screens exhibited highest NEP, DQE, and MTF at tube voltages higher than 55 kV and lower than 45 kV, whereas $La_2O_2S:Tb$ screens had better NEP, DQE, and MTF within the 45- to 55-kV range. Maximum NEP values were higher than 700 at 100–120 kV while maximum DQE(0) was 0.314 at 80 kV. $Gd_2O_2S:Tb$ screens are more efficient for high X-ray tube voltage applications (e.g., abdominal imaging, chest radiography, lumbar spine radiography, CT) and for very low voltage applications (e.g., mammography). $La_2O_2S:Tb$ screens are useful for medium-range X-ray voltages (e.g., pediatric radiography).

Key words Phosphor · Screen X-ray · Efficiency · MTF · Detective quantum efficiency

Introduction

Phosphors are materials used in medical imaging detectors to convert X-rays into optical signal. The intrinsic physical properties of phosphors, such as effective atomic number, energy of K-absorption edge, activator type, and density affect numerous parameters which are crucial in medical imaging. These parameters express the capability of a phosphor-based imaging detector to

extract diagnostic information from the X-ray beam transmitted through the human body. The definition of the parameters is based on: (a) the efficiency of a phosphor material to absorb incident radiation and convert its energy into emitted light [1, 2, 3, 4, 5, 6, 7, 8, 9, 10]; and (b) the capability to form images of high diagnostic information content [5, 6, 10, 11, 12, 13, 14, 15]. In the first case parameters such as absolute efficiency, relative efficiency, luminescence efficiency, gain, sensitivity, and

speed have been defined. On the other hand, information content has been evaluated by parameters such as spatial resolution, image contrast, noise, and signal-to-noise ratio (SNR).

In the present study the imaging performances of two of the most efficient phosphors, namely $\text{Gd}_2\text{O}_2\text{S:Tb}$ and $\text{La}_2\text{O}_2\text{S:Tb}$ as well as $\text{Gd}_2\text{O}_2\text{S-La}_2\text{O}_2\text{S}$, mixtures in various percentages, were studied and were compared. $\text{Gd}_2\text{O}_2\text{S:Tb}$ and $\text{La}_2\text{O}_2\text{S:Tb}$ differ in their effective atomic number, K-absorption edge, and density, but they have the same type of activator. Due to these differences, $\text{Gd}_2\text{O}_2\text{S:Tb}$ should be expected to perform better at relatively high diagnostic X-ray tube voltages, whereas $\text{La}_2\text{O}_2\text{S:Tb}$ performs better at lower voltages. The purpose of this study was to determine the range of tube voltages at which each phosphor is more efficient and, additionally, to investigate whether $\text{Gd}_2\text{O}_2\text{S-La}_2\text{O}_2\text{S}$ mixtures exhibit high performance in a wider range of diagnostic voltages than pure $\text{Gd}_2\text{O}_2\text{S}$ and $\text{La}_2\text{O}_2\text{S}$. This should provide information concerning the optimum use of each phosphor in various imaging applications.

The following imaging parameters were experimentally and theoretically evaluated:

1. The light emission efficiency [1, 2, 3, 4, 5, 6, 7, 8, 9, 10, 16], which was evaluated by determining the number of emitted photons (NEP) of light per incident X-ray
2. The modulation transfer function (MTF), which describes the variation of image contrast with spatial frequency and expresses spatial resolution [5, 10, 11, 12, 13, 14].
3. The detective quantum efficiency (DQE), which expresses the transfer of the SNR from the input to the output of an imaging system [6, 10, 11, 12, 13, 14, 15, 17].

Commercial intensifying screens which contain $\text{Gd}_2\text{O}_2\text{S:Tb-La}_2\text{O}_2\text{S:Tb}$ mixtures of specific percentage have been investigated in previous studies [6, 7, 8, 15]; however, in this paper the study was extended to include a larger variety of mixture percentages. Additionally, MTF and spatial frequency dependent DQE were experimentally and theoretically examined.

Materials and methods

The phosphor materials were supplied in powder form, by Derby Luminescents Ltd. (Code numbers GT1016 and LT133 for $\text{Gd}_2\text{O}_2\text{S:Tb}$ and $\text{La}_2\text{O}_2\text{S:Tb}$, respectively). The mean size of the powder grains was approximately 7 μm . Grain size affects both emission efficiency and spatial resolution [5, 11, 16, 18]; however, sizes in the range from 5 to 10 μm are generally accepted as a satisfactory compromise between emission efficiency and spatial resolution [5, 18]. The phosphors were used in the form of layers (screens) prepared in our laboratory [9, 10, 19, 20, 21, 22] with

various coating weights ranging from approximately 25 to 180 mg/cm^2 , which are often used in various types of X-ray imaging applications. Preparation was performed by sedimentation of the phosphor powder on fused silica substrates. Three types of screens were prepared: (a) screens which use 100% $\text{Gd}_2\text{O}_2\text{S:Tb}$ phosphor, (b) Screens which use 100% $\text{La}_2\text{O}_2\text{S:Tb}$ and 3. Screens which use 50% $\text{Gd}_2\text{O}_2\text{S:Tb}$ and 50% $\text{La}_2\text{O}_2\text{S:Tb}$ [22]. In all cases NaSiO_3 was used as binding material between the phosphor grains and the phosphor packing density was of approximately 50%, which is similar to that of commercially available phosphor screens. The screens were irradiated by X-rays using X-ray tube voltages from 40 to 120 kV. Tube voltage was checked using an RMI model 240 multifunction meter. The X-ray beam was filtered by an additional aluminum filter of 20 mm in order to simulate the effect of patient's body on X-ray beam.

NEP determination

To determine the number of emitted light photons per incident X-ray, first the light intensity I_L (or light energy flux, expressed in $\mu\text{W m}^{-2}$) emitted by the screens was measured by means of a photomultiplier (EMI 9558 QB) coupled to an electrometer (Cary 401). Data obtained by the electrometer were converted into light intensity (energy per unit of area and time) using manufacturer's photosensitivity data [9, 10, 19, 20, 21, 22]. Secondly, the exposure rate X (mR s^{-1}), related to the incident X-ray beam, was determined by a PTW ionization chamber dosimeter (type no. 23333); exposure measurements were performed during a second irradiation, under the same exposure conditions, except that the screen was replaced by the ionization chamber. (In all cases the reproducibility of the generator was within 4%.) In addition, optical emission spectra produced by the excited screens were measured using an Oriel 7440 grating monochromator. All these measurements were used to calculate the light emission efficiency, in number, $N\Phi$, of emitted light photons per incident X-ray, by the formula:

$$N\Phi = \frac{N_L}{N_X} = \frac{\left[\frac{I_L}{h\nu} \right]}{X\alpha(X,\Phi)} \quad (1)$$

where N_L is the total number of emitted light photons per unit of area and time when N_X X-ray photons are incident per unit of area and time on the surface of the screen; $h\nu$ is the energy of a light photon determined by the emission spectra measurements; and $\alpha(X, \Phi)$ is a coefficient converting exposure X into X-ray photon fluency Φ (photons per unit of area) [12]. Experimental uncertainties in NEP determination were of the order of 4%.

MTF determination

The modulation transfer function of each screen was determined following the square wave response function (SWRF) method, which has been explicitly described in previous studies [10, 19, 21, 22, 23, 24, 25]. The screens were used in combination with the Agfa Curix Ortho GS radiographic film. An MTF lead test pattern (type 53 of Nuclear Associates), which comprises lead line pairs with spatial frequencies ranging from 2.5 to 100 lp/cm , was placed in front of each screen. The frequency range of this pattern is appropriate for all X-ray imaging applications except for mammography; however, it has been previously employed for mammographic screen-film evaluation [26]. After screen irradiation, the images of the test pattern obtained on the films were digitized by a Microtec Scan maker II SP (24-bit color 1200 \times 1200 dpi) scanner. The test pattern was placed so that its line pairs were at right angles to the

Fig. 1 Variation of the number of emitted light photons per incident X-ray as a function of phosphor coating weight for $\text{Gd}_2\text{O}_2\text{S:Tb}$, $(\text{Gd,L a})_2\text{O}_2\text{S:Tb}$, and $\text{La}_2\text{O}_2\text{S:Tb}$ phosphors measured at 50 kVp. Points represent experimental data and solid lines model calculations

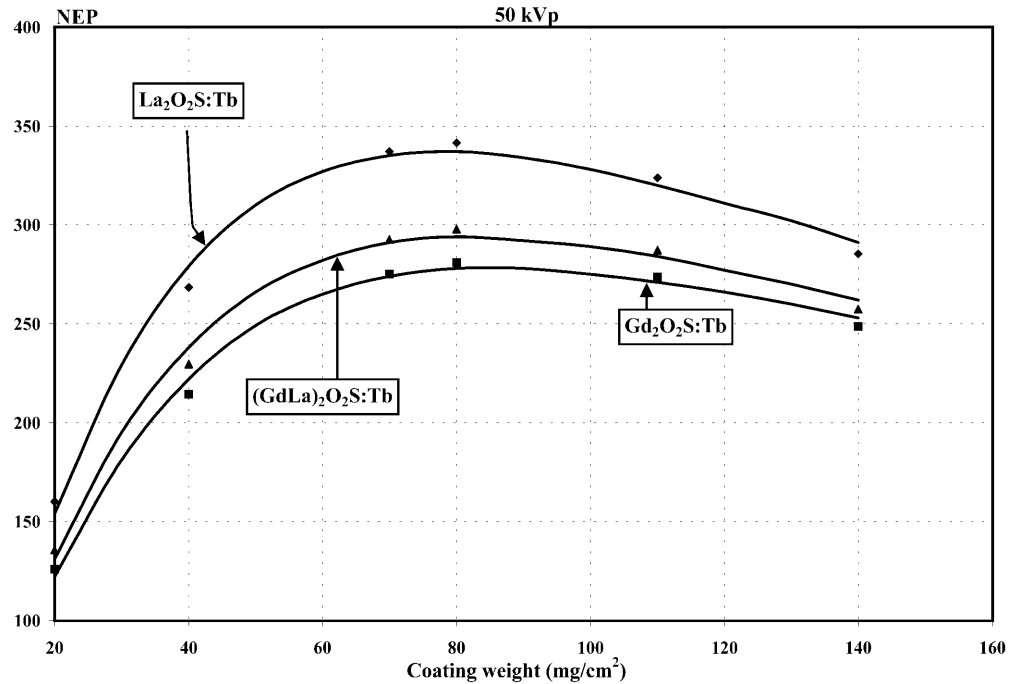


Table 1 X-ray to light conversion efficiency and attenuation coefficients

Phosphors	σ (cm^2/g)	β	η_c
$\text{Gd}_2\text{O}_2\text{S}$	30	0.03	0.20
$\text{La}_2\text{O}_2\text{S}$	30	0.03	0.18
$(\text{GdLa})_2\text{O}_2\text{S}$	30	0.03	0.19

scanning direction. In this way the SWRF was obtained from the digitized pattern images as image density variations across lines vertically directed with respect to the lines of the pattern. Sixty-four successive density variations were selected and averaged to eliminate noise. The MTF was then calculated by the formula of Coltman [19, 21, 23, 24, 25], which gives the MTF as a function of SWRF. This calculation, however, includes the MTF of the scanner and of the film. To obtain the screen MTF the data were corrected by dividing with the MTF of the scanner, whereas the film's MTF was considered equal to unity for frequencies up to 100 lp/cm [14, 19, 21]. The MTF uncertainties were between 0.7%, at low spatial frequencies and thin screens, and 3% at high frequencies and thick screens.

DQE determination

The detective quantum efficiency is defined as the square of the SNR characterizing a medical image divided by the square of the signal-to-noise ratio characterizing the incident X-ray beam. In the present study DQE was determined using a formula (see Appendix) based on NEP and MTF data:

$$\text{DQE} = \left[\frac{\text{SNR}_{\text{out}}}{\text{SNR}_{\text{in}}} \right]^2 = \frac{N_x N_\Phi^2 \text{MTF}^2}{\text{NPS}} \quad (2)$$

where NPS is the noise power spectrum associated with the light emitted by the phosphor. It is shown (see Appendix) that NPS can be determined as a function of N_x , N_Φ , MTF, and the number m_L of light photons emitted per absorbed X-ray photon:

$$\text{NPS} = N_x N_\Phi \left[m_L \text{MTF}^2 \right] + N_x N_\Phi \quad (3)$$

The number m_L can be calculated as the ratio of the emitted light photons N_L to the number of absorbed X-rays; the latter is calculated by considering exponential absorption of X-rays. The X-ray total mass energy absorption coefficient (in cm^2/g) of the phosphors was used which was calculated from data on corresponding coefficients of the chemical elements La, Gd, O, and S [27].

Theoretical calculations

The NEP, MTF, and DQE can be theoretically calculated employing the theoretical models of Hamaker [27], Ludwig [3, 19, 22, 25], and Swank [19, 25, 29]. These models describe the aforementioned parameters in terms of intrinsic physical properties of the phosphor materials, namely: the total mass energy absorption coefficient μ (in cm^2/g); the intrinsic X-ray to light conversion efficiency η_c ; and the coefficients related to the attenuation (absorption and scattering) of the light produced inside the phosphor screen (see Appendix). The equations of the models were used to fit the experimental data [30]. The fitting procedure was performed as follows:

1. The coefficients of X-ray absorption were calculated for each phosphor as described in the DQE section.
2. The intrinsic X-ray to light conversion efficiency for $\text{La}_2\text{O}_2\text{S:Tb}$ (0.18) and for $\text{Gd}_2\text{O}_2\text{S:Tb}$ (0.20) were obtained from previous studies [19]. In these studies data obtained under cathode ray excitation [31] were initially used. It is accepted that intrinsic conversion efficiencies under X-ray or cathode ray excitation do

Fig. 2 Experimental modulation transfer function (MTF) data for $Gd_2O_3:S:Tb$, $(Gd,La)_2O_3:S:Tb$, and $La_2O_3:S:Tb$ phosphors measured at 50 kVp

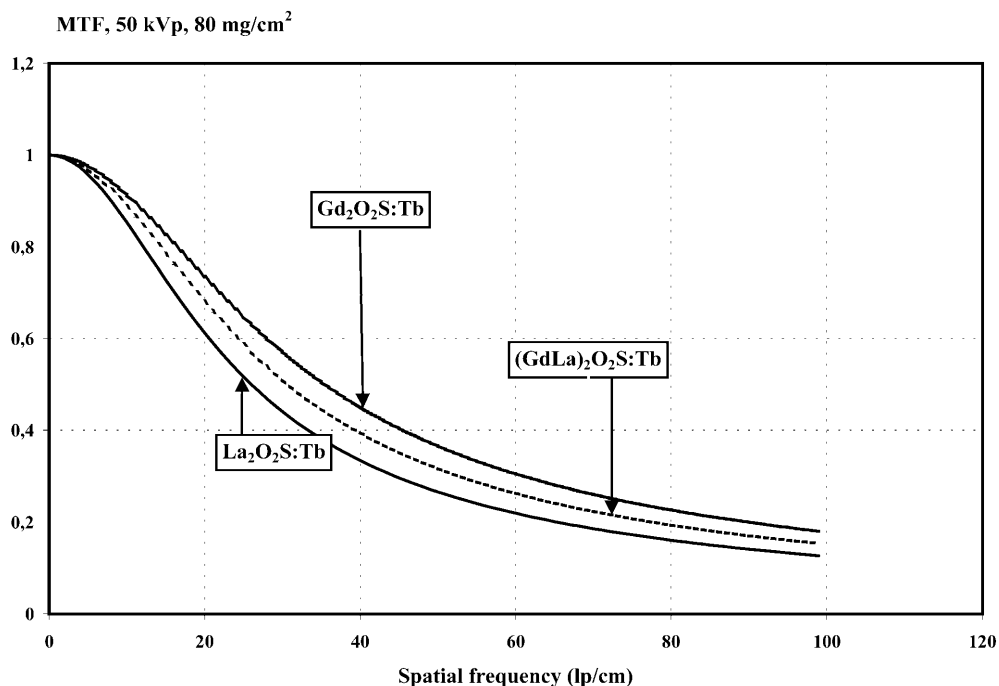
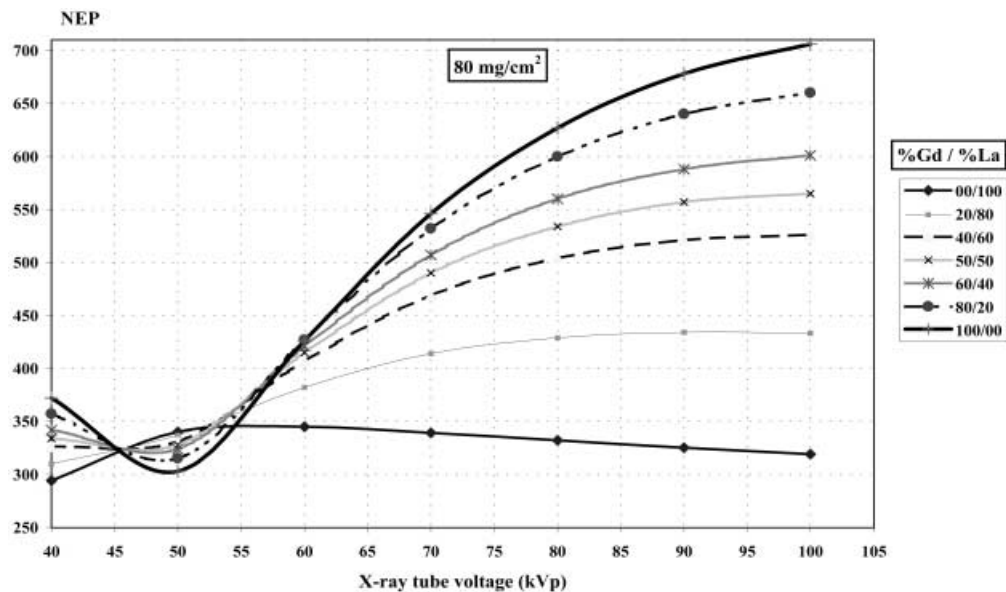


Fig. 3 Variation of number of emitted photons per incident X-ray (NEP) with X-ray tube voltage for various Gd_2O_3 - La_2O_3 mixtures of 80 mg/cm^2 coating weight



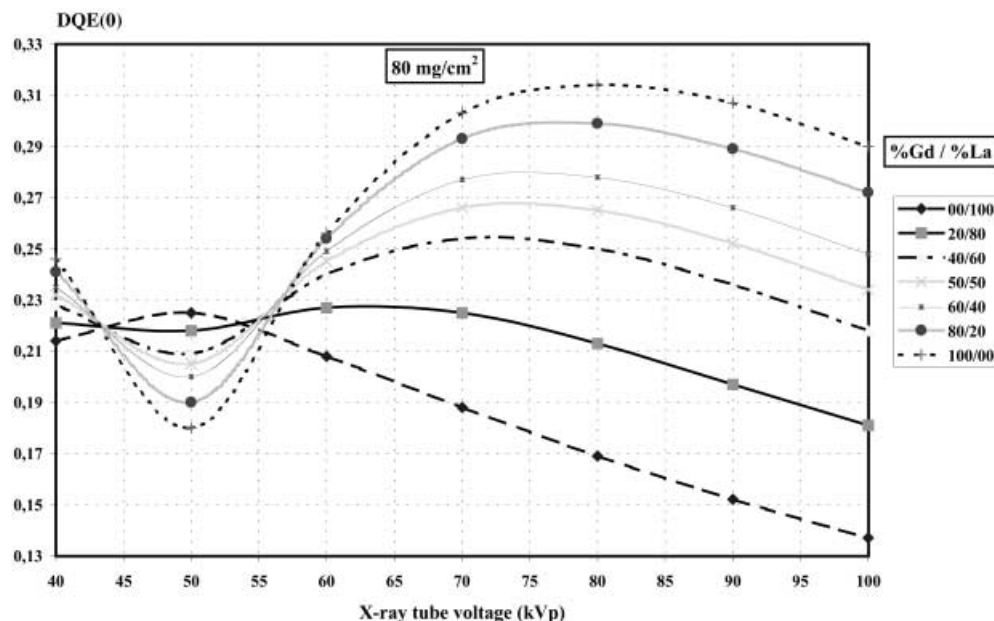
not differ significantly [4], since they depend on intrinsic phosphor properties and on temperature. The latter was practically constant during experiments; however, it was finally found that X-ray excitation values were higher. In the case of $(Gd_{0.5}La_{0.5})_2O_3:S:Tb$ this efficiency was taken to be equal to the mean value (0.19) of the two other materials [22].

3. The values of the coefficients related to light attenuation were allowed to vary so that best matching between the curves derived by the models and the experimental curves was obtained. The fitting technique followed the Levenberg-Marquard method [30].

The model equations were used to predict NEP, MTF, and DQE of phosphor screens prepared from mixtures of $Gd_2O_3:S:Tb$ and $La_2O_3:S:Tb$ in various Gd/La proportions ranging from 80–20% to 20–80%. For each mixture the calculation was performed considering the following assumptions:

1. The coefficients of X-ray absorption and the intrinsic X-ray to light conversion efficiencies of the various phosphor mixtures were calculated as the weighted average corresponding to the proportions of pure Gd_2O_3 and La_2O_3 involvement in each mixture.

Fig. 4 Variation of detective quantum efficiency (DQE) with X-ray tube voltage for various $Gd_2O_2S-La_2O_2S$ mixtures of 80 mg/cm^2 coating weight



2. The coefficients of light attenuation were kept constant and equal to those found by the fitting to the experimental data. The values of these coefficients were found approximately equal for the three experimental phosphors. This was expected since the wavelengths (spectra) of the emitted light photons and the size of the phosphor grains, which determine the phosphor's light attenuation properties, were very close in value in all phosphors.

Results and discussion

Figure 1 shows the variation of light emission efficiency (NEP) with screen coating weight measured at 50 kV for the three phosphors used in the experiments. Points represent experimental data, whereas solid lines represent fitted curves obtained by calculations according to the theoretical model (see Appendix) [3, 28, 29]. As it is observed the number of emitted light photons increases with screen coating weight up to a value around 80 mg/cm^2 and decreases slightly thereafter. The shape of the curves is due to the simultaneous effect of X-ray detection efficiency. Best curve fitting to the experimental results was obtained for the values of light attenuation coefficients shown in Table 1. It is noted that the phosphor ranking depicted in Fig. 1 is only valid within the voltage region from 45 to 60 kV. For voltages outside this range phosphor ranking was reversed, with $Gd_2O_2S:Tb$ showing higher NEP values.

Figure 2 shows MTF curves measured by the SWRF method [19, 23, 24, 25]. The MTF decreases with increasing spatial frequency. In contrast to what was observed in the case of NEP measurements, $Gd_2O_2S:Tb$ exhibited higher MTF values than the two other phosphors. The superiority of the MTF of $Gd_2O_2S:Tb$ is ex-

plained by considering the density of this material (7.43 g/cm^3). For a given coating weight, screens prepared from a high-density material are thinner than lower-density screens; thus, MTF is improved. Similar MTF curves were found at all X-ray tube voltages considered in this study and this also holds for the curves shown in Fig. 2, obtained at 50 kV. Experimental and theoretical results concerning DQE variation with coating thickness are not shown because the shape of curves was very similar to that shown in Fig. 1 for emission efficiency curves. This is explained by considering that DQE is directly proportional to the number of emitted light photons $N\Phi$, and hence similar reasoning may be applied to describe the variation of DQE values. The values of DQE peaked at 80 kVp and 80 mg/cm^2 , attaining a value of 0.312. This value is accurate within the limits of experimental errors [5, 6] and is also within the limits of values published by previous studies [6, 14, 15] on commercial systems.

Figure 3 shows the variation NEP with increasing X-ray tube voltage for various $Gd_2O_2S:Tb-La_2O_2S:Tb$ phosphor mixtures in varying proportions. As it is observed, the number of emitted light photons depends strongly on the proportions of Gd_2O_2S and La_2O_2S involved in the mixture. In the case of pure Gd_2O_2S phosphor (curve 100/00 in Fig. 3), the number of light photons decreases with tube voltage until 50 kVp, exhibiting a minimum value, and increases thereafter. This minimum value increases with decreasing Gd proportion in the mixture. In the 45- to 53-kV range, pure La_2O_2S phosphor exhibited best performance. In addition, the proportion of Gd and of La in the mixture affects the shape of the curves as follows: For voltages

Fig. 5 The NEP data for various 80 mg/cm^2 $\text{Gd}_2\text{O}_2\text{S}$ - $\text{La}_2\text{O}_2\text{S}$ mixtures and X-ray tube voltages

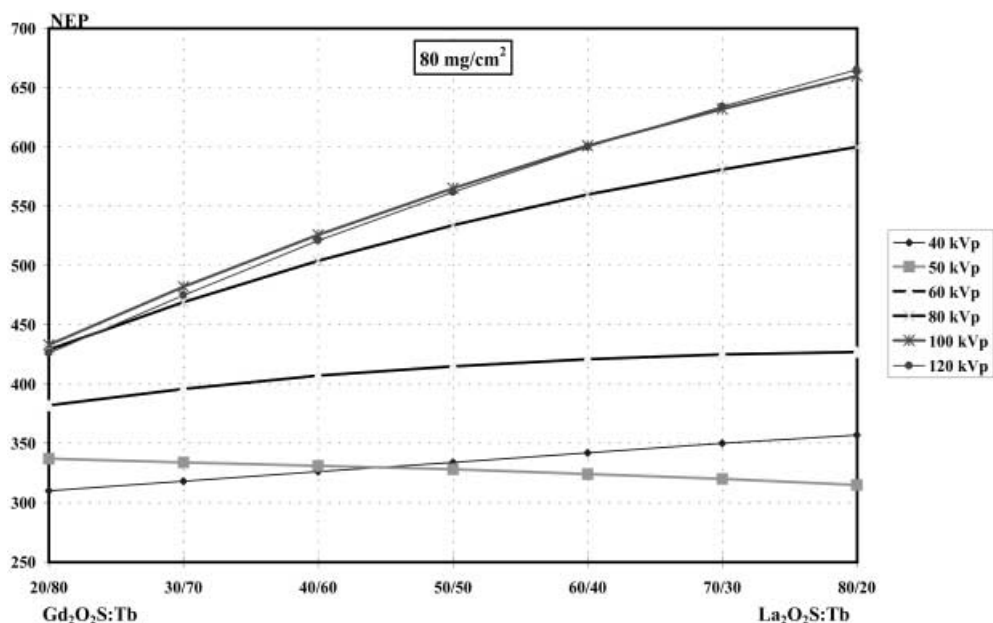
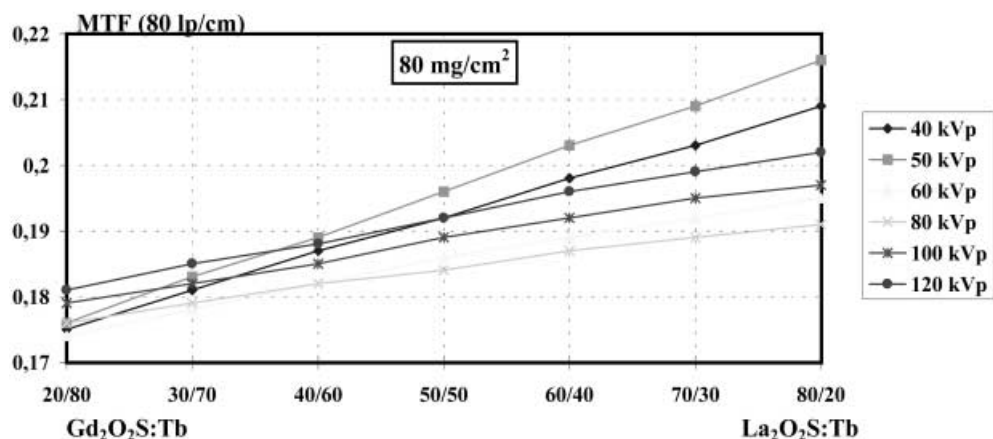


Fig. 6 The MTF data at 80 lp/cm spatial frequency for various 80 mg/cm^2 $\text{Gd}_2\text{O}_2\text{S}$ - $\text{La}_2\text{O}_2\text{S}$ mixtures and X-ray tube voltages

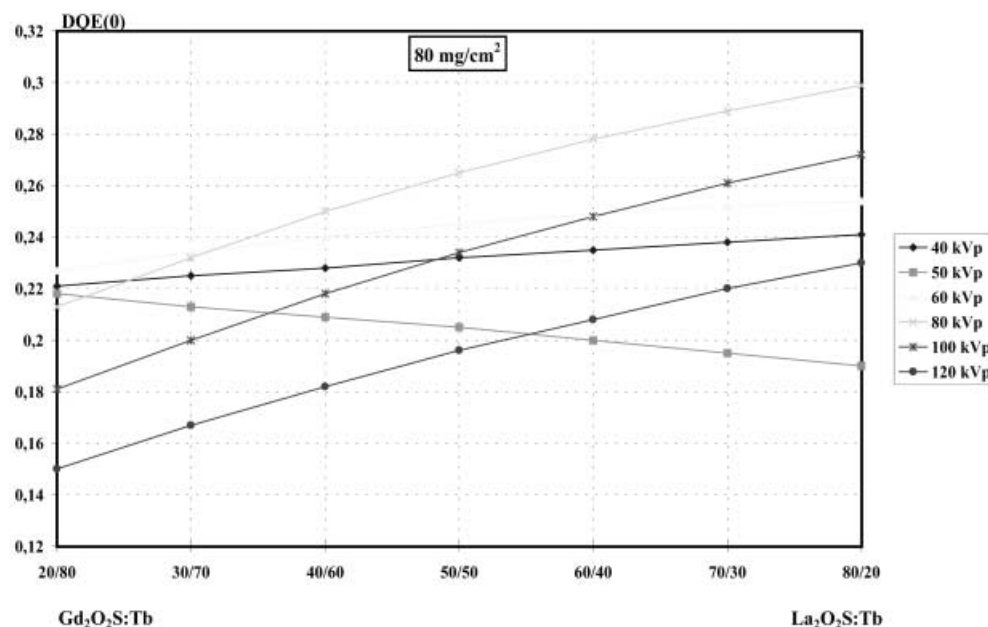


higher than 50 kV the emission efficiency of pure $\text{Gd}_2\text{O}_2\text{S}$ starts to increase continuously due to the presence of the K-shell absorption edge of Gd at 50.2 keV. As tube voltage increases to values higher than 50 kV, increasingly more X-ray photons acquire energies higher than 50 keV and thus they are easier absorbed by the Gd atoms; hence, higher intensities of light photons are produced and emitted. This behavior becomes less prominent when the $\text{Gd}_2\text{O}_2\text{S}$ proportion decreases with respect to $\text{La}_2\text{O}_2\text{S}$. In the range of voltages from 45 to 53 kV (around 50 kV), the number of emitted photons increases with increasing proportion of La atoms in the phosphor. This is explained by the fact that the K-absorption edge of lanthanum lies at 39 keV. Hence, when X-ray tube voltage is higher than 39 kVp, photons with energies from 39 to 50 keV are easier absorbed by lan-

thanum atoms. This increases the efficiency of $\text{La}_2\text{O}_2\text{S}$, which thus exceeds that of $\text{Gd}_2\text{O}_2\text{S}$ after 45 kVp; however, it must be taken into consideration that a fraction of the energy carried by photons exceeding the K-absorption edge is remitted within the phosphor, in the form of K-fluorescent radiation [32]. A large part of this radiation, amounting up to 31% for $\text{Gd}_2\text{O}_2\text{S}$, which is just above its K-edge [33], may escape the phosphor without contributing to light creation.

Figure 4 shows the variation of the zero frequency detective quantum efficiency ($\text{DQE}(0)$) with X-ray tube voltage for screens of 80 mg/cm^2 and various Gd/La proportions. At low and medium X-ray tube voltages, the shape of the DQE curves is similar to the emission efficiency curves (see Fig. 3). The DQE exhibits a minimum DQE value for the pure $\text{Gd}_2\text{O}_2\text{S}$ phosphor at

Fig. 7 The DQE data for various 80 mg/cm^2 $\text{Gd}_2\text{O}_2\text{S-La}_2\text{O}_2\text{S}$ mixtures and X-ray tube voltages



50 kV, whereas in the range from 43 to 55 kV the pure $\text{La}_2\text{O}_2\text{S}$ phosphor showed the highest DQE performance; however, for tube voltages in the range 70–80 kV, the shape of curves becomes different from the corresponding NEP curves. The DQE tends to decrease rapidly with voltage, indicating that at higher X-ray energies the role of quantum noise is more important than at medium (60–80 kV) or low energies (< 40 kV). This behavior may also be justified from Eqs. (2) and (3). The number (m_1) of light photons emitted per absorbed X-ray, which is in the denominator of Eq. (2), is expected to increase with tube voltage. This is because larger number of light photons are produced when larger amounts of X-ray energy are deposited within the phosphor mass. Additionally, high-energy X-rays are more penetrating; thus, they are absorbed closer to the output screen surface and light photons are easier transmitted through the phosphor. On the other hand, the number of emitted photons per incident X-ray ($N\Phi$), which is in the numerator of Eq. (2), exhibits a slight variation with tube voltage at voltages higher than 80 kV; hence, SNR and DQE show a tendency to decrease at high voltages.

Figures 5, 6, and 7 show the variation of light emission efficiency, MTF, and DQE, respectively, with the ratio of Gd/La proportions. In all cases data shown are determined at various X-ray tube voltages so that optimum “phosphor mixture-tube voltage” combinations can be obtained. The MTF values correspond to the frequency of 80 lp/cm, which is a high frequency, and thus these data express the spatial resolution of the screens. As is shown in the three figures, except for the cases of emission efficiency and DQE curves at 50 kVp,

in all other cases, the performance level of the phosphors increases with increasing Gd proportion in the mixture. On the contrary, at 50 kV, and in a range of voltages around this value, the emission and DQE performance levels increase with increasing La proportion.

Conclusion

From the aforementioned results it is concluded that materials which exhibit high effective atomic number, high density, high X-ray to light conversion efficiency, and a K-absorption edge within the diagnostically useful X-ray energies, such as $\text{Gd}_2\text{O}_2\text{S:Tb}$, are very effective as X-ray imaging detectors. The presence of other materials in the X-ray detector may only be justified in cases when X-ray energies higher than the K-absorption edge of this material are used. Hence, detectors with $\text{Gd}_2\text{O}_2\text{S:Tb}$ or high Gd proportion are suitable for diagnostic applications using high tube voltages (e.g., abdominal imaging, chest radiography, lumbar spine radiography, CT) and for applications using very low tube voltages (e.g., mammography). On the other hand, detectors with $\text{La}_2\text{O}_2\text{S:Tb}$ are more suitable for medium voltage applications (e.g., pediatric radiography). It is noted, however, that when considering the presence of the K-absorption edge, the fraction of re-emitted X-ray fluorescent photons that escape the phosphor should be taken into account. For instance, in the case of $\text{Gd}_2\text{O}_2\text{S}$ phosphor and for incident X-ray energies just above the energy of the K-edge, this fraction may amount up to 31% [33] of the incident energy.

Appendix

Theoretical light emission efficiency

Light emission efficiency was theoretically evaluated considering that it is the product of the following quantities [3, 5, 9, 10, 28, 29]:

$$N_{\Phi} = \eta_Q \eta_C G_L(a, s) \left[\frac{\bar{E}}{\bar{E}_{\lambda}} \right] \quad (A1)$$

where η_Q is the X-ray quantum detection efficiency (QDE), expressing the fraction of incident X-ray quanta detected by the screen, which is approximately given by:

$$\eta_Q = 1 - e^{-\mu T}, \quad (A2)$$

where μ is the mass attenuation coefficient of the phosphor for X-rays calculated using published data [27] and T is the screen-coating weight; η_Q is the intrinsic X-ray to light conversion efficiency, giving the fraction of absorbed X-ray energy converted to light within the phosphor material; $G_L(a, s)$ is the light transmission efficiency, expressing the fraction of light produced that reaches the screen output [3, 5, 9, 10, 25, 28, 29], with a and s being the coefficients of light absorption and light scattering, and \bar{E} is the mean energy of X-rays determined by the relation:

$$\bar{E} = \frac{\int_0^{E_0} \Phi(E) E dE}{\int_0^{E_0} \Phi(E) dE} \quad (A3)$$

where E_0 is the maximum X-ray energy, numerically equal to the X-ray tube voltage, and $\Phi(E)$ is the spectral distribution of X-rays, as given by Storm [34, 35].

\bar{E}_{λ} is the mean energy of light photons determined by:

$$\bar{E}_{\lambda} = \frac{\int \Phi_L(E_{\lambda}) E_{\lambda} dE_{\lambda}}{\int \Phi_L(E_{\lambda}) dE_{\lambda}} \quad (A4)$$

where Φ_L is the optical emission spectrum of the phosphor, determined experimentally.

Theoretical MTF

$G_L(a, s)$ has also been expressed [25, 29] as a function of spatial frequency f . In this case, MTF is expressed as:

$$\text{MTF}(f) = \frac{N_{\Phi}(f)}{N_{\Phi}(0)} = \frac{\int_0^{E_0} \Phi(E) \eta_Q \eta_C G_L(a, s, f) E dE}{\int_0^{E_0} \Phi(E) \eta_Q \eta_C G_L(a, s, 0) E dE} \quad (A5)$$

Detective quantum efficiency

The detective quantum efficiency has been previously expressed [10, 13, 36] by the formula:

$$\text{DQE} = N_X \left[\frac{dN_L}{dN_X} \right]^2 \frac{\text{MTF}^2}{\text{NPS}} \quad (A6)$$

The ratio dN_L/dN_X is equal to the number of emitted light photons per incident X-ray $N\Phi$. Thus:

$$\text{DQE} = N_X N_{\Phi}^2 \frac{\text{MTF}^2}{\text{NPS}} \quad (A7)$$

where [36]:

$$\text{NPS} = N_L [m_L \text{MTF}^2] + N_L$$

and from Eq. (1) it follows (see also Eq. (3)):

$$\text{NPS} = N_X N\Phi [m_L \text{MTF}^2] + N_X N\Phi \quad (A8)$$

It is noted that X-ray phosphors are detectors producing an output optical signal (light photons), which is determined by the energy of the incident X-ray beam (energy fluency); hence, the input SNR should be determined by the incident X-ray energy fluency. However, as has been demonstrated [17], the signal-to-noise ratio of an ideal detector, which captures all the information conveyed by the beam ($\text{DQE} = 1$), is equal to the mean number of incident photons (photon fluency). Hence, the incident X-ray photon fluency can be used as the SNR_{in} in the DQE calculation in a real detector, since, by definition, DQE expresses the degradation of input information (SNR_{in}) in real imaging detectors.

Acknowledgements This study is dedicated to the memory of Prof. G.E. Giakoumakis, leading member of our team, whose work on phosphor materials has inspired us to continue.

References

1. Hertz R H (1956) The spectral quantum and energy-efficiency of calcium tungstate X-ray intensifying screens. Br J Appl Phys 7: 182
2. Grum F, Costa LF, Donovan JL (1969) Measured light-emission efficiency and quantum yield for X-ray screens and phosphors. J Opt Soc Am 59: 848
3. Ludwig GW (1971) X-ray efficiency of powder phosphors. J Electrochem Soc 118: 1152

4. DePoorter JA, Brill A (1975) Absolute X-ray efficiencies of some phosphors. *J Electrochem Soc* 122: 1086
5. Morlotti R (1975) X-ray efficiency and modulation transfer function of fluorescent rare earth screens, determined by the Monte Carlo method. *J Photon Sci* 23: 181
6. Dick CE, Motz JW (1981) Image information transfer properties of X-ray fluorescent screens. *Med Phys* 8: 337
7. Venema HW (1979) X-ray absorption, speed, and luminescence efficiency of rare earth and other intensifying screens. *Radiology* 130: 765
8. Vyborny CJ, Metz CE, Doi K (1980) Relative efficiencies of energy to photographic density conversions in typical screen-film systems. *Radiology* 136: 465
9. Kandarakis I, Cavouras D, Panayiotakis GS, Triantis D, Nomicos CD (1998) Europium-activated phosphors for use in X-ray detectors of medical imaging systems. *Eur Radiol* 8: 3137
10. Kandarakis I, Cavouras D, Panayiotakis GS, Triantis D, Nomicos CD (1997) An experimental method for the determination of spatial frequency dependent detective quantum efficiency (DQE) of scintillators used in X-ray imaging detectors. *Nucl Instr Meth Phys Res A* 399: 335
11. Curry TS, Dowdey JE, Murry RC (1990) Luminescent screens. In: Christensen's physics of diagnostic radiology. Lea and Febiger, London, pp 118–136
12. Johns HE, Cunningham JR (1983) Diagnostic radiology. In: The physics of radiology. Thomas, Springfield, Illinois, pp 557–669
13. Dainty JC, Shaw R (1974) Detective quantum efficiency, signal to noise ratio, and the noise-equivalent number of quanta. In: Image science. Academic Press, New York, pp 152–188
14. Beutel J, Mickewich DJ, Issler SL, Shaw R (1993) The image quality characteristics of a novel ultra-high-resolution film/screen system. *Phys Med Biol* 38: 1195
15. Ginzburg A, Dick CE (1993) Image information transfer properties of X-ray intensifying screens in the range from 17 to 320 keV. *Med Phys* 20: 1013
16. Lindström J, Carlsson GA (1999) A simple model for estimating the particle size dependence of absolute efficiency of fluorescent screens. *Phys Med Biol* 44: 1353
17. Sandborg M, Carlsson GA (1992) Influence of X-ray spectrum, contrasting detail and detector on the signal to noise ratio and detective quantum efficiency in projection radiography. *Phys Med Biol* 33: 1245
18. Yaffe MJ, Rowlands JA (1997) X-ray detectors for digital radiography. *Phys Med Biol* 42: 1
19. Kandarakis I, Cavouras D, Panayiotakis G, Agelis T, Nomicos C, Giakoumakis G (1996) X-ray induced luminescence and spatial resolution of $\text{La}_2\text{O}_3\text{:Tb}$ phosphor screens. *Phys Med Biol* 41: 297
20. Cavouras D, Kandarakis I, Bakas A, Triantis D, Nomicos CD, Panayiotakis GS (1998) An experimental method to determine the effective luminescence efficiency of scintillator-photodetector combinations used in X-ray medical imaging systems. *Br J Radiol* 71: 766
21. Cavouras D, Kandarakis I, Prassopoulos P, Kanellopoulos E, Nomicos CD, Panayiotakis GS (1999) A method to evaluate the performance of X-ray imaging scintillators by means of the brightness-sharpness index (BSI) *Acta Radiol* 40: 211
22. Cavouras D, Kandarakis I, Nomicos CD, Bakas A, Panayiotakis GS (2000) Measurement of the $(\text{Gd},\text{La})_2\text{O}_3\text{:Tb}$ phosphor efficiency for X-ray imaging applications. *Radiat Meas* 32: 5
23. Coltman JW (1954) The specification of imaging properties by response to a sine wave input. *J Opt Soc Am* 44: 468
24. Barnes GT (1979) The use of bar pattern test objects in assessing the resolution of film/screen systems. In: Haus AG (ed) The physics of medical imaging recording system measurements and techniques. American Association of Physicists in Medicine, New York, pp 138–151
25. Cavouras D, Kandarakis I, Panayiotakis G, Evangelou EK, Nomicos CD (1996) An evaluation of the $\text{Y}_2\text{O}_3\text{:Eu}^{3+}$ scintillator for application in medical X-ray detectors and image receptors. *Med Phys* 23: 1965
26. Bunch CP, Huff KE, Van Metter R (1987) Analysis of the detective quantum efficiency of a radiographic screen-film combination. *J Opt Soc Am A* 4: 902
27. Storm E, Israel H (1967) Photon cross-sections from 0.001 to 100 MeV for elements 1 through 100. Report LA-3753, Los Alamos Scientific Laboratory, University of California
28. Hamaker H (1947) Radiation and heat conduction in light-scattering material. *Philips Res Rep* 2: 55
29. Swank RK (1973) Calculation of modulation transfer functions of X-ray fluorescent screens. *Appl Opt* 12: 1865
30. Press WÇ, Flannery BP, Teukolsky SA, Vetterling WT (1990) Numerical Recipes in C: The Art of Scientific Computing, Cambridge University Press, Cambridge, pp.540–547.
31. Alig RC, Bloom S (1977) Cathodoluminescent efficiency. *J Electrochem Soc* 124: 1136
32. Chan HP, Doi K (1983) Energy and angular dependence of X-ray absorption and its effect on radiographic response in screen-film systems. *Phys Med Biol* 28: 565
33. Boone JM, Seibert JA, Sabol JM, Tecotzky M (1999) A Monte-Carlo study of X-ray fluorescence in X-ray detectors. *Med Phys* 26: 905
34. Storm E (1972) Calculated bremsstrahlung spectra from thick tungsten targets. *Phys Rev A* 5: 2328
35. Tucker DM, Barnes GT, Chakraborty DB (1991) Semi-empirical model for generating tungsten target X-ray spectra. *Med Phys* 18: 211
36. Shaw R, Van Metter R (1984) An analysis of the fundamental limitations of screen-film systems for X-ray detection. *Proc SPIE* 454: 128